

Supplementary Materials for

3D meshes of carbon nanotubes guide functional reconnection of segregated spinal explants

Sadaf Usmani, Emily Rose Aurand, Manuela Medelin, Alessandra Fabbro, Denis Scaini, Jummi Laishram, Federica B. Rosselli, Alessio Ansuini, Davide Zoccolan, Manuela Scarselli, Maurizio De Crescenzi, Susanna Bosi, Maurizio Prato, Laura Ballerini

Published 15 July 2016, *Sci. Adv.* **2**, e1600087 (2016)

DOI: 10.1126/sciadv.1600087

This PDF file includes:

- Supplementary Materials and Methods
- fig. S1. Illustration of the permutation test to assess the statistical significance of the synchrony between the bursting activities of two cocultured explants.
- fig. S2. Organotypic spinal slices cultured on 2D MWCNT substrates and on 3D-PDMS scaffolds.
- fig. S3. Extracellular voltage transients represent evoked or spontaneous synaptic, action potential-mediated activity.
- fig. S4. Directionality analysis of spinal neuronal process outgrowth.
- fig. S5. Immune reaction over time to CNF scaffolds implanted into the adult rat visual cortex as a pilot study.
- References (56–61)

Supplementary Materials

Supplementary Materials and Methods

Carbon nanotubes three-dimensional frame and spinal cord organotypic culture preparation

Carbon nanotube three-dimensional frames (3D CNF) were obtained from Prof. Maurizio De Crescenzi's laboratory (52). As previously reported (52, 54, 55), manufactured carbon nanotube freestanding frameworks were three-dimensional meshes of self-assembled, interconnected large multi-walled carbon nanotubes (MWCNT). MWCNTs were up to 0.4 μm in diameter and up to hundreds of μm in length, 3D CNF were obtained by chemical vapor deposition (CVD) as described in previous works (52, 54, 55). 3D CNFs were characterized by a bulky stiffness, measured by a compressive load cell, of about 5 kPa, a value within the range of the reported tissue stiffness for rodent and human brains (from 0.1 to 20 kPa) (56). 3D CNFs also displayed high electrical conductivity (52). The bulky 3D scaffolds were cut into thin square slices (3 mm \times 4 mm lateral size; 250–400 μm thickness) and then secured on standard glass coverslips (Kindler) by PDMS (Sylgard® 184 silicone elastomer, Dow-Corning, US) cured at 150°C for 15 minutes. Thereafter substrates were cleaned under low-pressure air plasma for 5 minutes (PDC-32G Plasma Cleaner, Harrick Plasma) and UV sterilized for 20 minutes before use.

Organotypic cultures were obtained from spinal cords of E12 embryonic mouse (C57Bl) as previously reported (8, 21, 26). Pregnant mice were sacrificed by CO₂ overdose and decapitation and fetuses delivered by caesarean section. Isolated fetuses were decapitated and their backs were isolated from low thoracic and high lumbar regions and transversely sliced (275 μm) with a tissue chopper. After dissecting the spinal cord slices from the surrounding tissue, two of them were mounted on control glass coverslips (Control) or on 3D CNF attached to the coverslips, and arranged at a similar distance in both conditions, to interface slice growth. In both conditions, slices were embedded into a thick matrix obtained by chicken plasma (Rockland) and thrombin (Sigma) clot. Slices were cultured in plastic tubes with 1.5 mL medium containing 67% DMEM (Invitrogen), 8% sterile water for tissue culture, 25% fetal bovine serum (Invitrogen), and 25 ng/mL nerve growth factor (Alomone Laboratories); osmolarity, 300 mOsm; pH 7.35. The tubes were kept in a roller drum rotating 120 times per hour in an incubator at 37°C in the presence of humidified atmosphere, with 5% CO₂. Slices were cultured for 10–17 days. To ensure

homogeneous experimental conditions between the two analyzed populations (Control and 3D CNF double explants), for electrophysiological and immunofluorescence experiments pairs of organotypic spinal explants with inter-slice distance (measured between the center of the two explants by bright field imaging) exceeding the 0.8–2.5 mm distance-range were discarded.

Electrophysiological recordings

Coverslips with spinal cultures were placed in a recording chamber, mounted on an upright microscope (Leica DM LFS), and superfused with Krebs' solution containing (in mM): 152 NaCl, 4 KCl, 1 MgCl₂, 2 CaCl₂, 10 HEPES, and 10 Glucose. The pH was adjusted to 7.4 with NaOH. All experiments were performed at room temperature (RT; 20–22°C). Simultaneous extracellular recordings were obtained from the ventral area of each explant using low resistance glass micropipettes (4–6 MΩ) filled with KCl (20 mM) solution; microelectrodes were positioned with micromanipulators (Luigs and Neumann SM1, Germany) and advanced into spinal tissue manually by micro-steps. The electrodes were usually placed in close proximity (20–100 μm) to the ventral fissure, as this area, on both sides of the spinal cord, has been described as the prominent source of rhythmic activity in spinal slice cultures (57, 58). Voltage transients could be attributed to synaptic activity and action potential firing. Bursting activity was completely suppressed by bath-applied 6-Cyano-7-nitroquinoxaline-2,3-dione (CNQX; 10 μM) plus tetrodotoxin (TTX; 1 μM) in 100% of cases (n=13 explants, Control and 3D CNF; fig. S3B). The recorded signals were amplified (Axopatch 1D; Axon Instruments) and the offset of the traces was neutralized by current injection through the amplifier. Signals were recorded using the Clampex 8.2 software (pClamp suite, Axon Instruments) and acquired digitized (Digidata 1322A, Axon Instruments) at 10 kHz, filtered at 2 kHz and stored on a PC. Disinhibited rhythmic bursts were obtained by bath co-application of strychnine and bicuculline (1 μM and 20 μM, respectively)(20). Extracellular electrical stimulation was performed by placing a low-resistance patch pipette containing external bath solution in the dorsal horn of one explant, ipsilateral to the ventral area being recorded. Short current pulses (200 μs) of various amplitudes (i.e. the amplitude able to elicit the appearance of a voltage burst response in the ipsilateral ventral region in 100% of stimuli; ranges 100–500 μA; sample in fig. S3A), were delivered by a STG4002 stimulator (Multichannel Systems).

Recordings were off-line, lowpass-filtered at 20 Hz for spontaneous activity analysis, and for disinhibited bursts analysis at 100 Hz (cross-entrainment analysis) or 3 Hz (cross-correlation and inter-event interval analysis). To evaluate the frequency of spontaneous voltage transients (in the absence of any pharmacological treatment or electrical stimulation), only the events with peak amplitudes above threshold (set to three times the baseline noise) were included. Disinhibited bursts occurrence was evaluated by measuring the mean inter-event interval (IEI; i.e. the time between the beginning of one burst and the beginning of the following one; >25 bursts for each measure).

We further assessed the synchrony between the bursting activities of the two explants in each pair by computing the Pearson correlation coefficient between the two voltage time series as follows: in the experiments in which the Control slices were compared to 3D CNF slices (see Fig. 3A-D) or to 2D MWCNTs and 3D-PDMS (see fig. S2), the statistical significance of the correlation coefficient was determined by performing a permutation test (see fig. S1). For each pair of time series, we randomly sampled time windows of consecutive data points of size $s = N/5$ (where N is the total number of data points of the time series), and, for each window, we computed the Pearson correlation coefficient between the resulting chunks of time series (see the example in fig. S1A, where the dashed lines indicate the extremes of a randomly sampled time window and the gray traces indicate the portions of the time series that were used to compute the correlation coefficient). This procedure was repeated 10^4 times, thus yielding 10^4 correlation coefficients that were averaged to obtain an estimate of the correlation between the two time series (for the sample of time series shown in fig. S1A, the resulting average correlation coefficient is shown by the red line in the plot of fig. S1C). This value was compared to the null distribution of correlation coefficients that was obtained by taking time windows of consecutive data points of the same size s as before, but with the onsets of the time windows that were independently, randomly sampled for the two time series (see, as an example, the gray portions of the time series in fig. S1B). Again, this procedure was repeated 10^4 times, yielding the distribution of correlation coefficients that one would expect to observe if the voltage signals recorded from a pair of explants happened to correlate purely by chance, even in absence of synchrony (see the histogram in fig. S1C). By measuring how likely it was for the values of this null distribution to be larger or equal than the real correlation coefficient (i.e., for the values of

the histogram in fig. S1C to be larger than the red line), it was possible to understand whether the correlation between the pair of time series was significantly larger than expected by chance (with $P=0.05$). Since, in general, two time series could be anti-correlated as well as correlated, the same test was applied to the left tail of the null distribution, in case the measured correlation coefficient was negative (i.e., we checked how likely it was for the values of the null distribution to be smaller or equal than the measured correlation coefficient). This procedure allowed for determining what fraction of co-cultured slices exhibited a significantly synchronous bursting activity, for all the tested conditions. The resulting fractions of significantly synchronous slices were then compared by performing a homogeneity test with the chi-squared method (shown in Fig. 3D). For the stimulation-based experiments (Fig. 3E-G), the bursting activities of two explants in a pair were considered synchronous, when the magnitude of their CCF was larger than 0.5.

Immunofluorescence labeling and confocal imaging of spinal slice explants

Following electrophysiological recordings, spinal organotypic cultures were fixed with 4% formaldehyde (prepared from fresh paraformaldehyde; Sigma) in PBS. Coverslips were rinsed with PBS. Free aldehyde groups were quenched in 0.1 M glycine in PBS for 5 minutes. The samples were incubated for 30 minutes in a blocking solution (5% BSA, Sigma, 0.3% Triton X-100, Carlo Erba, 1% Fetal Bovine Serum, Gibco, in PBS), then incubated with anti- β -tubulin III primary antibody (rabbit polyclonal; 1:250, Sigma) and SMI-32 primary antibody (mouse anti-neurofilament H antibody, 1:200, Sternberger Monoclonals Inc.) diluted in PBS with 5% FBS at 4°C, overnight. After subsequent washing in PBS, samples were incubated in secondary antibodies (goat anti-mouse Alexa 488, Invitrogen, 1:500; goat anti-rabbit Alexa 594, Invitrogen, 1:500; DAPI, Invitrogen 1:500) for 2 h at room temperature. Following secondary antibody incubation, samples were washed in PBS and briefly rinsed with water and mounted on glass coverslips using Vectashield hardset mounting medium (Vector laboratories).

Images were acquired using Nikon C2 or Leica DMIRE2 Confocal microscopes, both equipped with Ar/Kr, He/Ne, and UV lasers. Images were acquired with a 40 \times or 63 \times oil objective (numerical aperture 1.4) using oil mounting medium (1.515 refractive index). Confocal sections were acquired every 1 μ m and the total Z-stack thickness was set such that all emitted

fluorescence was collected from the sample. In order to visualize the 3D CNF scaffold along with the immunolabeled components, the reflection mode setting (excitation with the 488 nm laser line and acquisition of the reflected signal in the 460–500 nm range) available in the Leica confocal microscope was utilized. Analysis and 3D reconstruction of the image Z-stacks were accomplished using one of the following softwares: NIS-Elements AR (Nikon), Volocity (PerkinElmer), and FIJI (<http://fiji.sc/Fiji>).

Analysis of fiber outgrowth morphology was performed by selecting random regions of 160 μm *per* 160 μm of visual field dimension at 40 \times magnification. To visualize and appreciate the difference in the 3D distribution of the neuronal processes in Control and 3D CNF networks, the three-dimensional extent of the processes was also visualized by color-coding for the thickness through which they extended; FIJI and MATLAB software packages were employed for this analysis. The Z-stacks of representative neuronal processes extensions were first viewed using FIJI and color-coded for the thickness by using the *Temporal-color code* command in the *Hyperstacks* section of the software. The images obtained were then visualized in MATLAB and the figure color-map was set such that for both conditions, the color depth demonstrated equal thickness, thus ensuring homogeneity in the color scheme in Control and 3D CNF. To quantify the distribution of neuron processes along the thickness of the image stack, 9 regions from 6 coverslips of Control and 14 regions from 5 coverslips of 3D CNF were compared. The thickness through which the immunolabeled processes were distributed was calculated (using FIJI) and the statistical differences between the datasets were assessed by Student's t test (after validation of variances homogeneity by Levene's test; Statistica software).

In order to rule out any possible discrepancy in the fluorescence emission due to the 3D scaffold, images of fluorescent beads (2 μm biodegradable micro-particles from Kisker, PBD-GF-2.0; a kind gift from Dr. Dan Cojoc, CNR-IOM, Trieste) deposited on glass and on 3D CNF were acquired using identical settings. The intensity of the fluorescence was analyzed using the Volocity software to confirm that the substrate did not produce any artifact in the emitted fluorescence signal.

Brain tissue implantation with 3D CNF

The implant consisted of a sharp-pointed cylinder (~2 mm length, 0.5 ± 0.2 mm in diameter) carved out of a larger 3D CNF scaffold and mounted on an electrode holder (ZIF-Clip[®], Tucker-Davis Technologies, USA). Scaffold stiffness was increased before carving procedure in order to facilitate the insertion of the material into the brain tissue. This stiffening was achieved by filling the scaffold with water-soluble polyethylene glycol (PEG), a biocompatible polymeric material commonly used for implants and hydrogels (59, 60). Briefly, the 3D CNF scaffold was dipped into melted PEG-4000 (Poly(ethylene glycol); 81240 from Sigma Aldrich, average MW 4,000 Da) at 65°C. PEG molecules permeate the scaffold, filling all empty spaces. The sample was allowed to cool to RT and shaped with a razor blade. To facilitate handling and positioning during the surgical procedure, the scaffold was fixed to the electrode holder using PEG.

All surgical procedures were performed on Wistar male rats (Harlan Laboratories), 3–6 months of age and weighing 450–550 gr. Anesthesia was induced and maintained with Isoflurane (2% in 100% O₂, Sigma Aldrich) administered via a nose cone throughout the procedure. Anesthetic depth was monitored by checking the absence of tail and paw reflexes. The anesthetized animal was placed in a stereotaxic apparatus (Narishige SR-5R, Japan) to measure the exact location of the craniotomy and the penetration site. Body temperature was maintained at 37°C with a thermostatically controlled heating pad (temperature control unit HB 101/2; Panlab/Harvard Apparatus, Barcelona, Spain) to avoid anesthesia-induced hypothermia. Heart rate and oxygen saturation level were constantly monitored via a pulse oxymeter (Pulsesense LS1P-10R, Nonin Medical Inc, Medair AB, Hudiksvall, Sweden). A square, 2 mm × 2 mm craniotomy was performed over the left hemisphere using a micro drill and the *dura mater* was removed, exposing the brain. Tissue adhesive (B. Braun Aeusculap, Germany) was applied on the inner perimeter of the craniotomy to prevent brain dimpling.

The PEG-stiffened 3D CNF scaffold was inserted at –4.5 mm from Bregma (in the anterior-posterior axis) and –3.5 mm in the medial-lateral axis. These coordinates refer, in the adult rat, to the visual cortex, specifically to the cortical junction between V2ML and V1 (61). 3D CNF scaffold was quickly placed into the cortex via a micro-drive at a speed of insertion of about 0.5 mm/s in order to prevent premature PEG melting. When the desired depth was reached, i.e. the

sponge penetrated the cerebral tissue for approximately its whole length (~2 mm in the dorsal-ventral axis), the craniotomy was filled with silicone (Kwik-Cast&Kwik-sil, World Precision Instrument, USA) in order to isolate the exposed brain tissue, and the whole skull surface covered by bone cement (Super Bond, C&B, USA).

Throughout the whole procedure, both rat eyes and cortex were periodically irrigated, using an ophthalmic solution (Epigel, CevaVetem, Italy), and a 0.9% NaCl saline solution, respectively. Atropine (1.5 mg/kg, subcutaneous) and Lactated Ringer's Solution (1 mL, subcutaneous) were administered every hour, to reduce secretions and maintain the animal's physiological state. Analgesic solution (Rymadyl; 5 mg/kg, intraperitoneal) and antibiotic (Baytril; 5 mg/kg, intramuscular) were administered to the rat via injection, immediately before the surgery and one hour prior to the end of the surgical procedure. Both solutions were administered following surgery via the animals' drinking water for three days post-surgery. Animals were monitored for recovery immediately after the surgery and at least 3 times per day for the first 72 h. We used a general distress-scoring sheet (Institutional Standards for the Care and Use of Animals in Research and after consulting with a veterinarian) to assess pain and distress in animals using physiological (appearance) and behavioral (natural and provoked behavior) parameters. For each parameter a numerical score starting from 0=normal and reaching 3=grossly abnormal is determined. An extra point is added for each 3 given. The provoked behavior was tested first after 72 h post-implantation. This method allows an objective monitoring of animals general conditions, to evaluate the need of analgesics or euthanization. All the animals used in the study did not show any sign of pain or distress (score=0). Following this 72 h period, animals were monitored once per day until sacrifice.

Brain tissue preparation, immunohistochemistry, image acquisition, and analysis

Animals were sacrificed at 4 weeks post-implantation and, in an exploratory longitudinal study, at five different post-implantation time points, as follows: 0 weeks (in which the animal was euthanized immediately after the implantation, "acute"), 1 week, 2 weeks, 4 weeks and 8 weeks. Animals were anesthetized with 5% chloral hydrate (7 mL/kg) and then perfused transcardially with 0.1 M PBS followed by 4% PFA in PBS. Brains were removed, postfixed for 24 h at 4°C, and cryoprotected in 15% sucrose in PBS at 4°C for 24 h and then in 30% sucrose in PBS at 4°C

for at least 24 h. Finally, brains were embedded in optimal cutting temperature (OCT) compound (Tissue-Tek), frozen at -20°C , and cryosectioned horizontally in 25 μm thick sections.

Tissue-Tek was removed by PBS washing and tissue sections were incubated 5 min in glycine 0.1 M and blocked in 3% BSA, 3% FBS, 0.3% Triton X-100 in PBS for 30 min at room temperature followed by incubation overnight at 4°C with primary antibodies (mouse anti-GFAP, 1:200, Sigma; rabbit anti-Iba1, 1:400, Wako; rabbit anti- β -tubulin III, 1:250, Sigma; mouse anti-NeuN, 1:100, Millipore; mouse anti-CD68/ED1, 1:100, AbD Serotec; rabbit anti-CX3CR1, 1:200, Sigma) in 5% FBS in PBS. After washing in PBS, sections were incubated in secondary antibodies (goat anti-rabbit Alexa 594, 1:500, Invitrogen; goat anti-mouse Alexa 488, 1:500, Invitrogen; DAPI, 1:200, Invitrogen) in 5% FBS in PBS for 2 h at room temperature. Sections were mounted on glass coverslips using Vectashield hard mounting medium (Vector Laboratories).

We measured the brain tissue reaction at specific time after implants by markers for reactive astrocytes, with glial fibrillary acidic protein (GFAP), for microglia with ionized calcium-binding adaptor protein-1 (Iba1), and for neurons (β -tubulin III; NeuN). In order to quantify GFAP and Iba1 labeling, fluorescence images were acquired using a Leica DM6000 upright microscope with a $10\times$ dry objective. Identical binning, gains and exposure times were used for all images of the same marker. Image analysis was performed using the FIJI software. Different quantification methods were used for GFAP and Iba1 labeling. For GFAP, eight regions of interest (ROIs; $100\ \mu\text{m} \times 500\ \mu\text{m}$) were drawn at random intervals around the implant, starting from the edge of the implant and extending $500\ \mu\text{m}$ into the surrounding tissue. Within each ROI, three intensity profile lines were selected blindly in order to obtain a fluorescence intensity profile as a function of distance from the implant edge. To account for variations in labeling, the fluorescence intensity in the contralateral hemisphere was defined as the background intensity for each brain section and normalized to 1(37). The mean intensity profile for each animal was calculated for each micron of 0– $150\ \mu\text{m}$ from the implant edge. Because differences in GFAP intensity were within a maximum of $50\ \mu\text{m}$ from the implant, the data from 0– $150\ \mu\text{m}$ were further normalized to the mean intensity for 51– $150\ \mu\text{m}$.

In the longitudinal study (n=1 animal per time point; fig. S5) the mean GFAP fluorescence intensity in the 0–50 μm ROI was increased from 4 to 8 weeks post-implantation (1.07 ± 0.13 and 1.05 ± 0.11 normalized intensity/ μm , respectively; n=56 and 80 ROIs) compared to 0, 1, and 2 weeks post implantation (0.94 ± 0.10 , 0.92 ± 0.14 , and 0.94 ± 0.12 normalized intensity/ μm , respectively; n=40 ROIs for 0 and 1 weeks, n=64 ROIs for 2 weeks; fig. S5A-B).

For Iba1 labeling, eight $100\ \mu\text{m} \times 500\ \mu\text{m}$ ROIs were selected starting from the edge of the implant and extending $500\ \mu\text{m}$ into the surrounding tissue. The background intensity threshold was defined for each tissue section using the Iba1 labeling intensity measured in the contralateral hemisphere in the same anatomical region as the implanted material. The area within each ROI with intensity above the background threshold was calculated.

In the longitudinal study, the Iba1 immunoreactivity was greatly increased at 1 week post-implantation compared to the acute/ 0 weeks (Iba1-positive area/total area: 0.34 ± 0.18 and 0.043 ± 0.02 , respectively; n=32 and 32 ROIs, fig. S5C-D). Furthermore, microglia cells were clearly invading the 3D CNF. At 2 and 4 weeks post-implantation, the Iba1 labeling was still increased compared to the acute/0 weeks post-implantation (Iba1-positive area/total area: 0.089 ± 0.06 , n=64 ROIs, $P=0.018$ and 0.16 ± 0.11 , n=40 ROIs); however, the reactivity at these time points was *reduced* compared to the 1 week post-implantation tissue, meaning that microglia surrounding the implanted material were primarily active in the first week following the implantation and then activation declined with time. This was further confirmed at 8 weeks post-implantation, in which the Iba1 labeling around the implant (Iba1-positive area/total area: 0.04 ± 0.03 , n=64 ROIs) returned to baseline condition.

In addition to the GFAP and Iba1 analysis of the animals at 4 weeks post-implantation, we analyzed the tissue for CX3CR1 and CD68/ED1, markers of inflammation and reactive astrocytes (data not shown). For this analysis, three $150\ \mu\text{m} \times 150\ \mu\text{m}$ ROIs were selected within each 3D CNF scaffold. The background intensity threshold was defined for each tissue section using the corresponding labeling intensity measured in the contralateral hemisphere in the same anatomical region as the implanted material. The area within each ROI with intensity above the background threshold was calculated. We performed this analysis on animals sacrificed at 4

weeks post-implantation. The average values obtained for CX3CR1 (CX3CR1-positive area/total area: 0.32 ± 0.23 , $n=18$ ROIs) and CD68/ED1 (CD68/ED1-positive area/total area: 0.12 ± 0.17 , $n=18$ ROIs) represent the 36% and 13% of the total amount of microglia cells (calculated in the same way based on Iba1 labeling), respectively, indicating a relatively low percentage of reactive microglia inside the 3D CNF scaffold. Moreover, CD68/ED1-positive cells were totally absent in the surrounding tissue.

Confocal images of brain tissue sections were acquired and processed using the same equipment and procedures as the spinal slice explants, as described above.

Scanning Electron Microscopy

3D CNF morphology was qualitatively assessed through scanning electron microscopy (SEM). Images were acquired collecting secondary electrons on a Gemini SUPRA 40 SEM (Carl Zeiss NTS GmbH, Oberkochen). Bare scaffolds were mounted on conductive double side carbon tape (Ted Pella, Inc., USA) and imaged at 5 keV.

Mechanical characterization

For compressive tests, cubic samples of 3D CNF scaffolds were used, with a dimension of 5 mm per side. Uniaxial micro-compression tests were conducted on a Galdabini SUN 500 apparatus. Before compressive testing, a 0.01 N preload was applied to ensure a complete contact between the sample and the two flat surfaces compressing it. A constant speed ($15 \mu\text{m/s}$) loading cycle was used with a load limit fixed at 10 N. After the limit was reached, we recorded discharging cycle to point out potential sample plastic deformation. Final peak displacement was about 3 mm. Scaffolds were indented using a 20 mm flat punch using a high sensitivity load cell for data collection (CTCA10K5 – AEP Transducers, Italy). Tests were operated at room temperature in air. Elastic data were determined by calculating the initial linear slope of the stress-strain curve.

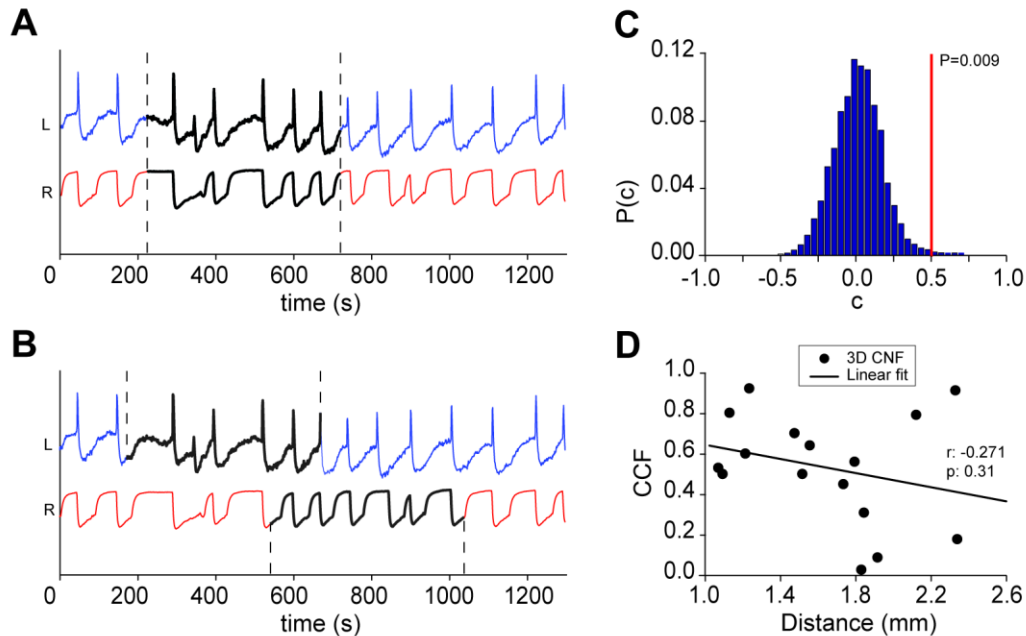


Figure S1. Illustration of the permutation test to assess the statistical significance of the synchrony between the bursting activities of two co-cultured explants.

A. Two example extracellular recordings (L, left slice; R, right slice) obtained from co-cultured slices that have been pharmacologically disinhibited. The recordings show rhythmic bursting activity, where the synchrony between the slices was determined by computing their Pearson correlation coefficient in time windows (10^4 distinct time windows) that were randomly sampled from the whole duration of the recording (a single example time window is shown delineated by the dashed lines). **B.** To obtain a null distribution of correlation coefficients expected to be observed by chance, the randomly selected time window (dashed lines) for one slice was shifted within the trace and compared for synchrony with a similar length time window (now at a different time point) for the second slice. This analysis was repeated 10^4 times to obtain a null distribution of the correlation coefficients. The figure shows one of such randomly chosen time windows (dashed lines) and the resulting portions of the recordings (gray traces) that were compared to determine the correlation coefficient. **C.** The figure shows the null distribution (histogram, blue) of correlation coefficients for a pair of slices produced by the randomization procedures described in **B**. The red line indicates the true correlation coefficient for the same slices determined as described in **A**. For the traces shown, the true CCF value is +0.5 (red line) and the probability of observing null distribution values equal to or larger than the actual correlation coefficient ($CCFs \geq 0.5$) was very low. Therefore, the bursting activity of the slices was significantly ($P=0.009$) more synchronous than expected by chance. **D.** The distance between the two slices (center of slice to center of slice, in mm) does not affect the cross-correlation coefficient (CCF) in 3D CNF samples (black line indicates the regression line, $r=-0.271$, $p=0.31$), indicating that sample synchrony is not determined by how far the slices are separated.

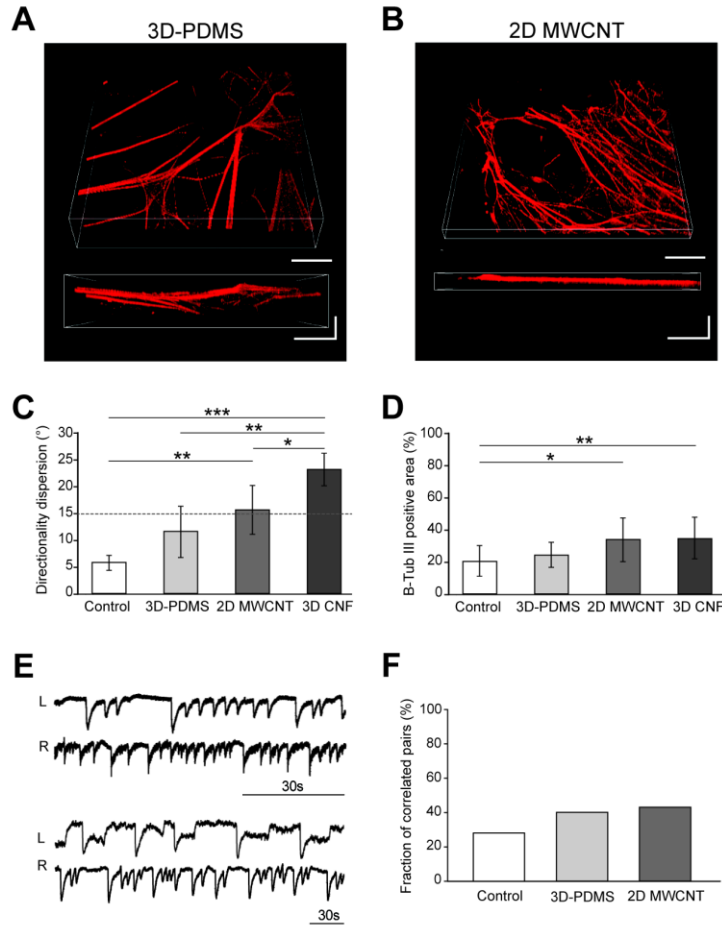


Figure S2. Organotypic spinal slices cultured on 3D-PDMS scaffolds and on 2D MWCNT substrates.

A and B. Confocal microscopy reconstruction depicting the three-dimensional growth of β -tubulin III-positive fibers on the 3D-PDMS scaffolds and on the 2D MWCNT substrates, respectively. Below, side views of reconstructions of these samples show neurites infiltrating through the z-axis on 3D-PDMS scaffolds (to a 126 μm depth), or fasciculated into bundles and flattening on 2D MWCNT substrates (to a 40 μm thickness). **C.** Histograms depict the average angle of dispersion of the fibers in Control, 3D-PDMS, 2D MWCNT, and 3D CNF samples. The lower angle of dispersion in Controls suggests that neurite fiber bundles are more oriented compared with 3D CNF, in which there is a high degree of dispersion, paralleling the mesh-like formation of the fibers (Control vs. 2D MWCNT $P=0.008$; Control vs. 3D CNF $P=0.000001$; 3D-PDMS vs. 3D CNF $P=0.003$; 2D MWCNT vs. 3D CNF $P=0.012$; overall significance determined by one-way ANOVA: $F(3,38)=12.24$, $P=0.000009$). **D.** Plots summarizing the average percentage of sample area from fiber reconstruction images positive for β -tubulin III immunofluorescence. These data suggest at the fiber density of the samples, but do not account for the dispersion of fibers into the third dimension. There were significant increases in β -tubulin III-positive area in CNT-containing samples over Controls (overall significance, $F(3,38)=3.99$, $P=0.015$; Control vs. 2D MWCNT $P=0.011$; Control vs. 3D CNF $P=0.004$). **E.** Representative LFPs of disinhibited bursts recorded simultaneously from paired slices grown on 3D-PDMS (top) and 2D MWCNT (bottom); note the absence of left-right correlation in these sample tracings. **F.** Plots of pooled data summarizing the mean fraction of correlated pairs detected in Controls, 3D-PDMS, and 2D MWCNT ($n=7, 5, 7$, respectively). These values did not significantly differ (Control vs. 3D-PDMS $P=0.68$; Control vs. 2D MWCNT $P=0.58$; 3D-PDMS vs. 2D MWCNT $P=0.92$).

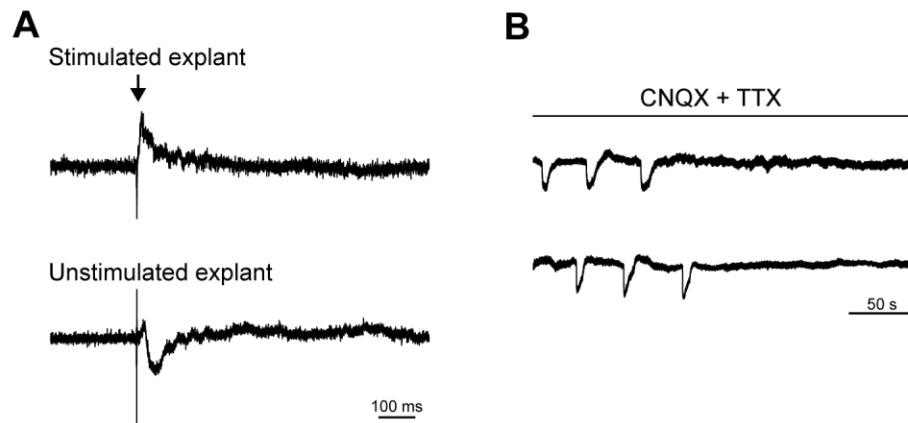


Figure S3. Extracellular voltage transients represent evoked or spontaneous synaptic, action potential mediated, activity.

A. Tracings of evoked LFPs recorded from the ventral horn of two co-cultured spinal explants in 3D CNF. The response to the dorsal electrical stimulation (arrow) is shown in the directly stimulated (top) and in the correlated (bottom) spinal slice. The delay between the application of electrical stimulation and the response onset in the directly stimulated explant was similar in both 3D CNF and Controls (6.2 ± 2.0 ms, $n=4$ 3D CNF; 6.4 ± 0.7 ms, $n=5$ Control). **B.** Bursting activity recorded in the presence of strychnine and bicuculline in Control slice pairs is completely suppressed by CNQX ($10 \mu\text{M}$) and TTX ($1 \mu\text{M}$) application.

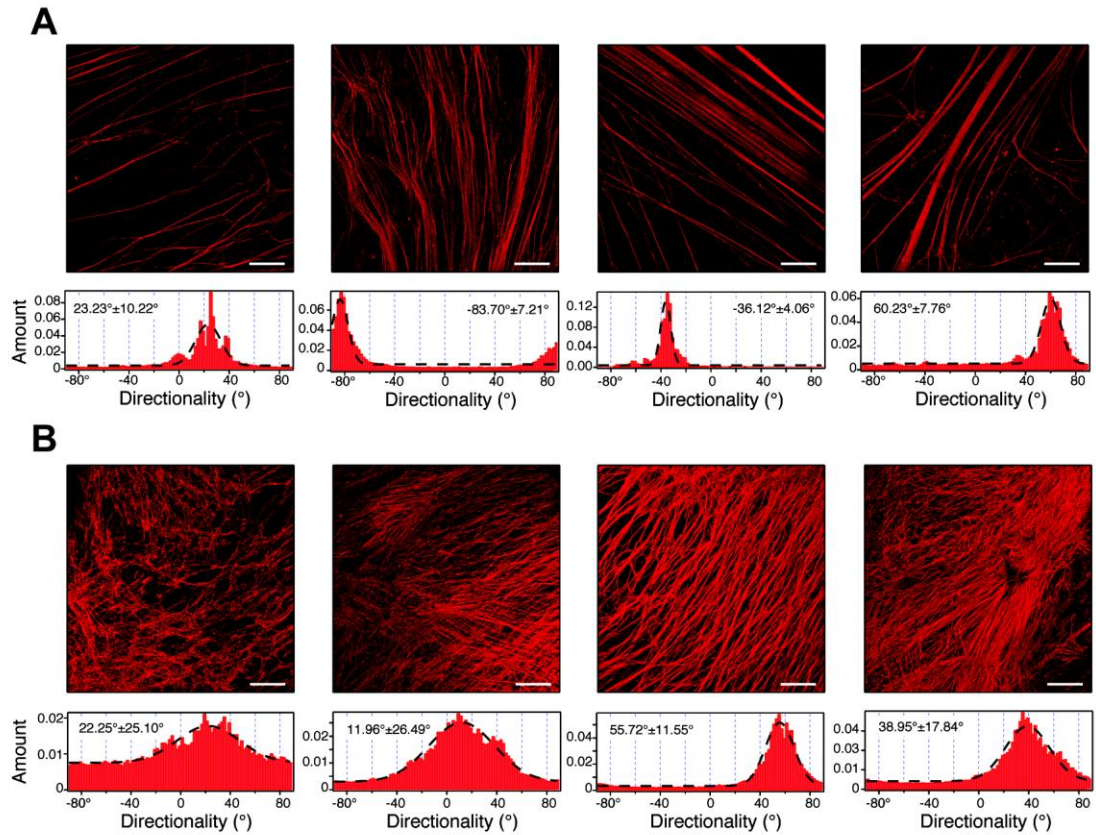


Figure S4. Directionality analysis of spinal neuronal processes outgrowth.

A. Confocal images representative of Control neuronal projection appearance (top, β -tubulin III stained; $n=4$ cultures) and corresponding fiber angular distributions (bottom); note that in the majority of cases the mean directionality dispersion is lower than 10° . **B.** Confocal images representative of 3D CNF neuronal projection appearance (top, β -tubulin III stained; $n=4$ cultures) and corresponding fiber angular distributions (bottom); note that in these samples the mean directionality dispersion is higher than 10° . Mean values and dispersion were calculated from Gaussian fitting (black dashed line) of fibers angular distribution and reported as histogram inset. We define a field as “oriented” if the direction dispersion is lower than 10° , otherwise it is defined as “random”. See SI Materials and Methods for details. Scale bars: $100\ \mu\text{m}$.

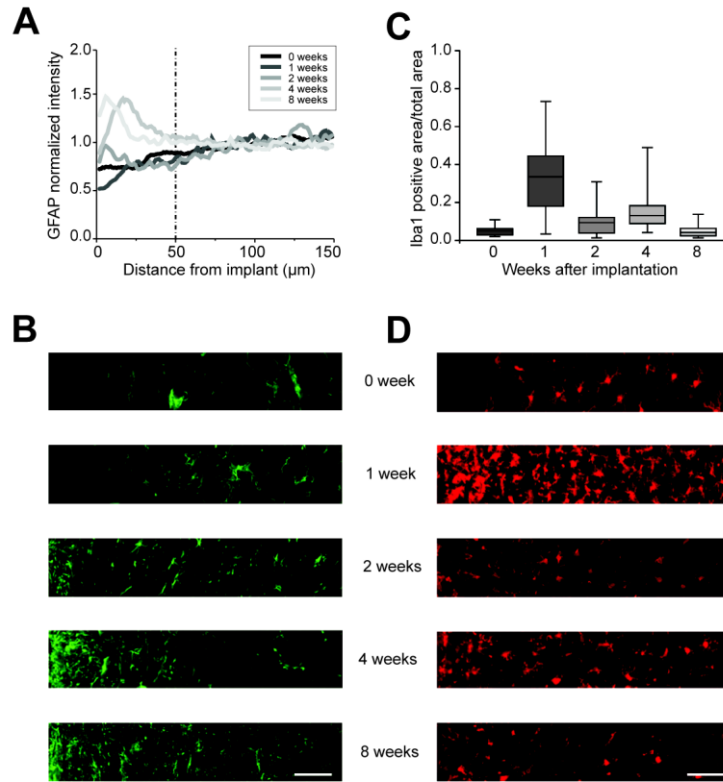


Figure S5. Immune reaction over time to CNF scaffolds implanted into the adult rat visual cortex.

A. GFAP fluorescence intensity profile in the surrounding tissue as a function of the distance from the edge of the implant. **B.** Representative images of the ROIs used for analysis, showing GFAP labeling (green) at the different time points post implantation; the edge of the CNF scaffold forms the left border of each image. **C.** Mean Iba1-positive area measured up to 500 μm from the edge of the implant. **D.** Representative images of ROIs demonstrating the Iba1 fluorescence labeling (red); the edge of the CNF scaffold forms the left border of each image. Scale bars in **B** and **D**: 50 μm .